Atomic structure of nanometer-sized amorphous TiO_2

Hengzhong Zhang,* Bin Chen, and Jillian F. Banfield
Department of Earth and Planetary Science, University of California Berkeley, Berkeley, California 94720, USA

Glenn A. Waychunas
Earth Sciences Division, Lawrence Berkeley National Laboratory, Berkeley, California 94720, USA

Amorphous titania (TiO_2) is an important precursor for synthesis of single-phase nanocrystalline anatase. We synthesized x-ray amorphous titania by hydrolysis of titanium ethoxide at the ice point. Transmission electron microscopy examination and nitrogen gas adsorption indicated the particle size of the synthesized titania is ~ 2 nm. Synchrotron wide-angle x-ray scattering (WAXS) was used to probe the atomic correlations in this amorphous sample. Atomic pair-distribution function (PDF) derived from Fourier transform of the WAXS data was used for reverse Monte Carlo (RMC) simulations of the atomic structure of the amorphous TiO_2 nanoparticles. Molecular dynamics simulations were used to generate input structures for the RMC. X-ray absorption spectroscopy (XAS) simulations were used to screen candidate structures obtained from the RMC by comparing with experimental XAS data. The structure model that best describes both the WAXS and XAS data shows that an amorphous TiO_2 particle consists of a highly distorted shell and a small strained anatase-like crystalline core. The average coordination number of Ti is 5.3 and most Ti-O bonds are populated around 1.940 Å. Relative to bulk TiO_2, the reduction of the coordination number is primarily due to the truncation of the Ti-O octahedra at the amorphous nanoparticle surface and the shortening of the Ti-O bond length to the bond contraction in the distorted shell. The pre-existence of the anatase-like core may be critical to the formation of single-phase nanocrystalline anatase in crystallization of amorphous TiO_2 upon heating.

I. INTRODUCTION

Titania (TiO_2) is a semiconductor [the band gap is 3.2 eV so many would call this an insulator as this is too large for meaningful Boltzmann population of the conduction band----however natural titania is always a semiconductor-GAW] material with applications in many fields, including medicine, cosmetics, electronics and chemical engineering. It is known that nanocrystalline anatase has higher photocatalytic activity than other titania nanophases and bulk titania [2001Gao]. However, sol-gel synthesis of nanocrystalline titania often results in a mixture of nano-anatase and brookite [2001nanolett]. Upon heating, the two nanophases transform to rutile [1999AmMiner, 2000JMR, 2000JPCB, 2007JPCC]. In previous work, we developed a two-steps route for synthesis of single-phase nanocrystalline anatase [2001nanolett]. First, amorphous TiO_2

precursor is produced via hydrolysis of titanium ethoxide at a low temperature. Then, heat treatment of the amorphous precursor produces single-phase nanocrystalline anatase.

Thermodynamically, anatase is more stable than rutile at sizes < ~ 14 nm [1998JMC, 2000JPCB]. However, anatase is only marginally more stable than brookite at sizes < ~ 11 nm [2000JPCB]). This means that in synthesis of nano-titania, brookite is likely to form together with anatase. Considering this, the formation of single-phase nano-anatase (rather than a mixture with brookite) from amorphous titania must be due to the formation kinetics rather than the thermodynamics. Kinetic studies show that the crystallization of nano-anatase from amorphous TiO_2 is initiated at the interfaces between precursor particles [2002ChemMater]. However, it is unclear why the precursor particles preferentially transform to anatase rather than brookite upon heating. Understanding the detailed atomic structure of amorphous titania should help to unveil the transformation mechanism at the atomic level, which will benefit optimization of the structure and properties of single-phase nano-anatase produced from amorphous TiO_2.

In previous studies, [**refs**] researchers have used x-ray absorption spectroscopy (XAS), including XANES (x-ray absorption near-edge structure) and EXAFS (extended x-ray absorption fine structure), to investigate the local atomic structures in nanometer-sized amorphous titania or very fine titania nanoparticles. For very fine (~ 3 nm) titania particles, Chen et al. gave a coordination number (CN) of 4.8 for Ti atoms based on their EXAFS fitting of the Ti- K-edge XAS data, though they concluded that the Ti sites are largely octahedral (CN = 6) [1997ChenLX_XAFS]. Later they showed that, for ~ 2 nm colloid titania particles, the coordination numbers of Ti atoms are 3.9 to 5.8 according to the EXAFS fitting [1999ChenLX.pdf]. They concluded that distortions in the TiO_2 structure are mainly located on the surface of the particles. Luca et al's EXAFS fitting also showed that small titania xerogels contain Ti in distorted coordination with contracted Ti-O bonds and probably reduced coordination number (CN < 6) [1998Luca_XAS_TiO2.pdf]. This seems consistent with Yeung's EXAFS fitting that showed that the Ti-O bond length is 1.93 Å and the coordination number of Ti is 4.5 for a ~ 3 nm TiO_2 sample [2002Yeung_TiO2XAS.pdf]. From deconvolution of the pre-edge peaks in the Ti K-edge XANES spectra of amorphous mesoporous titania, Yoshitake et al. concluded that 5- and 6-coordinated Ti atoms are coexisted in the sample, with their populations being 39% and 61%, respectively [2003Yosh_XAFS.pdf & 2002Yosh_XAFS.pdf]. Fernandez-Garcia et al. studied the structure of alkoxide-derived amorphous titania using both XAS and pair-distribution function (PDF) methods. Based on the pre-edge feature of the XANES spectra, they deduced that their samples contained 5-coordinated Ti atoms. However, their EXAFS fitting showed that the coordination number of Ti atoms is 6.2-6.7, and hence inconsistent with their XAS infererence [2007Fern_anaTiO2]. Petkov et al. studied the structures of sol-gel derived, thin film and bulk amorphous titania using x-ray/electron diffraction [1998Petk_amoTiO2_Imp-see.pdf]. Bulk structure models were used in their reverse Monte Carlo (RMC) simulations and from the RMC they concluded that their samples have brookite-like short-range atomic arrangements.

These previous studies generally pointed out the reduction of the Ti coordination number and the shortening of the Ti-O bond in amorphous (or ultrafine titania particles). However, a detailed atomic view, particularly of the surface, is still lacking. Such knowledge is essential since chemical and physical processes usually either take place on

particle surfaces, or are initiated there, and the numbers of atoms on amorphous nanoparticle surfaces constitute the majority. In this work, we measured the wide-angle x-ray scattering (WAXS) pattern of alkoxide-derived amorphous titania using a synchrotron radiation x-ray source, and calculated the atomic pair-distribution. Structure models were obtained from RMC by generating the best approximation of the PDF data. By comparing the simulated XAS spectra of these RMC models with the experimentally measured one, we were able to establish a structure model that best describes both the WAXS and XAS data. Structure characteristics of the amorphous titania (including surface and interior parts) were further analyzed using this structure model.
[at this pint I am wondering why you didn't use both the EXAFS and PDF with the RMC code, essentially requiring a best generation of both simultaneous? If you actually did that, then this needs rewording.-GAW]

II. EXPERIMENTAL

A. Synthesis and characterization of nanometer-sized amorphous TiO_2

Amorphous titania was prepared by hydrolysis of titanium ethoxide in water at 0 ^{o}C (cooled in a bath of ice + water). 29 mL water containing 4 drops of acetic acid was quickly added to a mixture of titanium ethoxide (21 mL; ACROS Organics, New Jersey) and ethanol (25 mL; AAPER Alcohol and Chemical Co., Kentucky) under stirring. The product was centrifuged and washed repeatedly with ethanol first and then with water, and then dried at ~ 80 °C. The dried sample (in powers) was kept in a sealed glass vial for experimental determinations.

The sample was examined by x-ray diffraction (XRD). A small amount of the sample was lightly ground [careful! Grinding can cause phase transformations-GAW] in acetone in a mortar with a pestle and then dispersed onto a low x-ray scattering background silica plate. The plate was loaded into the sample holder of an x-ray diffractometer (PANalytical X'Pert PRO) operated at 40 kV and 40 mA with a Co K_α radiation x-ray source (wavelength 1.7903 Å). The XRD pattern was collected in the 2θ range of 10-90 ^{o} with a scanning rate of 1°/min.

Transmission electron microscopy (TEM) characterization of the microstructure of the sample was done with a Philips CM200 high-resolution transmission electron microscope operated at 200 kV. A TEM specimen was prepared by adding a droplet of titania nanoparticles ultrasonically dispersed in water onto a carbon-coated copper TEM grid, followed by drying in air.

The surface area of the sample was determined via the BET method using nitrogen gas adsorption at 77 K, performed with an Accelerated Surface Area and Porosimetry System (Micrometrics ASAP2010).

B. Wide-angle x-ray scattering

WAXS measurements were performed at the high-energy beamline station 11-ID-C, Advanced Photon Source, Argonne National Laboratory (USA). The x-ray wavelength

was 0.10770 Å and the sample-to-camera distance was ~ 272 mm. The exact distance was calibrated using diffraction from a CeO_2 standard.

A thin layer of the titania sample was sandwiched between Kapton tape, and attached to a disk-like sample holder with an opening for x-ray transmission WAXS measurements. WAXS patterns were acquired at room temperature, with a q (scattering vector) range of 0.3 – 30 $Å^{-1}$ and a q step size of 0.01 $Å^{-1}$. The WAXS pattern was captured by an image plate detector, with integration of the circularly symmetric scattering pattern about the transmitted beam direction. The WAXS pattern of blank Kapton tape was also acquired for background subtraction. The structure factor, $S(q)$, of the sample was derived from the WAXS pattern after suitable data reduction [2004science]. The atomic PDF, G, of the titania sample was obtained as a function of radial distance (r) through Fourier transform of the structure factor: [2004Science]

$$G(r) = \frac{2}{\pi}\int_0^\infty q[S(q)-1]\sin(qr)dq \qquad (1)$$

C. X-ray absorption spectra

Ti K-edge (adsorption energy 4966 eV) XANES spectra of bulk anatase, bulk rutile and the titania sample were measured at Beamline stations 5-BM-D and 12-BM-B(**??**), Advanced Photon Source, Argonne National Laboratory (USA). One portion (weight) of the sample was mixed well with ~ 100 (**??**) portions (weight) of boron nitride (a low-background diluter). The mixture was then transferred into a rectangular-shaped sample window in a sample holder (~ 0.5 mm thick **??**), with one side of the window sealed with a piece of Kapton tape. The other side of the window was sealed using another piece of Kapton tape after loading the sample into the window. [need to fix this up- GAW] The measurements were done in transmission mode at room temperature. XANES spectra were collected over the photon energy range of 4965-5020 eV with a step increment varying between 0.2 - 1.4 eV/step. A smaller step increment was used for measuring the pre-edge features of the XAS spectra. *A **(xxxx ??)** monochromator was used for reduction of the contribution from higher harmonics.* [was this a detuning of the monochromator, or maybe a mirror was used? –GAW]The x-ray intensities before the sample, after transmission through the sample, and after subsequent transmission through a standard Ti foil were measured using ionization detectors. Photon energy was calibrated using the absorption spectra of the Ti foil.

III. COMPUTATIONAL MODELING

A. Molecular dynamics simulations

We used molecular dynamics (MD) simulations to generate input structures for RMC simulations of the structure of amorphous nano-TiO_2. For the purpose of comparison, we used two sets of interatomic potential functions of TiO_2 in the MD. The first set is the one developed by Matsui and Akaogi (MA) [1991Matin which each Ti and O atom carries a charge of +2.196 and -1.098, respectively, and the short-range

interatomic interactions are described by a Buckingham potential. The MA potentials have been used extensively in simulations of TiO_2 materials (e.g. [2005JPCB]). The second set is the one developed by Kim et al. (KIM) [1996Kimwherein each Ti and O atom carries a charge of +2.4 and -1.2, respectively, and the short-range interatomic interactions are described by a Morse potential.

MD simulations were performed using the parallel code DL_POLY [2001dlpoly]. Initial configurations for the MD were structures of 2 nm and 3 nm (diameter) anatase, brookite and rutile particles generated by cutting spheres from coordinates of their corresponding bulk phases. In general, the as-cut particles were not charge-balanced, and thus they were further neutralized by removing excess charged atoms on the surfaces. The MD simulations were carried out in the canonical ensemble (NVT ensemble) at 300 K for MD times of 100 – 500 ps at a step of $(2.0 – 5.0)\times10^{-5}$ ps. The MD times were long enough to ensure that all the MD systems were fully energetically and structurally relaxed, as indicated by the reaching of a steady state condition in the MD.

B. Reverse Monte Carlo simulations

In a classical Monte Carlo (MC) simulation of the structure of a material, some randomly chosen atoms of the material are moved in random directions for randomly assigned distances. If the energy of the formed new structure is lower than that before the move, the move is "good" and the new structure is accepted. Otherwise, the move is "bad" and the new structure is accepted with a probability of

$$p = \exp\left(-\frac{E_{after} - E_{before}}{RT}\right) \qquad (2)$$

where E is the molar energy of the material, R the gas constant and T the temperature. After iterating for a sufficient number of MC cycles, the energy of the material decreases to a point where it only fluctuates around a steady value. This energy-minimized structure is considered the most-probable one for the material. However, in RMC, rather than minimizing the energy of the material, the difference between an observed quantity and a calculated one is minimized through movements of the atoms of a model structure. In this work, the quantity is the atomic pair-distribution function.

In searching for structure models for the amorphous nano-TiO_2 using RMC, we used MD structures as initial input structures for the RMC. It was found that using an as-cut structure from bulk TiO_2 nanoparticle as the initial structure for the corresponding nanoparticle often caused the RMC to fail. This is because an as-cut structure is generally very far from the actual relaxed structure. The goodness of fit for an RMC structure simulation is measured by the difference between the calculated PDF and the experimental one, (χ^2), as defined below

$$\chi^2 = \frac{\sum_i \left[I_{i,expt} - (f \cdot I_{i,calc} + b)\right]^2}{\sigma^2} = \frac{residual}{\sigma^2} \qquad (3)$$

where $I_{i,\,expt}$ is the experimental PDF intensity at a measured scattering vector q_i, $I_{i,cala}$ is the calculated PDF intensity at the corresponding scattering vector, σ^2 is a parameter that controls the fraction of a "bad" move which are accepted, and *f* and *b* are respectively a scaling factor and a constant that are optimized in each move. In RMC, if a move of an atom causes χ^2 to decrease, then the new structure is accepted (i.e. a "good" move). Otherwise, if χ^2 increases (i.e. a"bad" move), the new structure is accepted with a probability of

$$p = \exp\left(-\frac{\chi^2_{after} - \chi^2_{before}}{2}\right). \qquad (4)$$

After iterating for sufficient RMC cycles, χ^2 will decrease to a point where it fluctuates around a steady value with no further significant structural changes.

In our RMC simulations, for each RMC step about 3 % atoms in the TiO_2 model structure were randomly chosen to move in random directions for random displacements of up to 0.08 Å. [why were these values chosen? –GAW] Only a small fraction of the atoms were chosen in each random move as use of larger fractions often results in inability to decrease the residual. Using a maximum displacement of 0.08 Å also avoided the breaking of Ti-O bonds during each RMC step, a likely unphysical process. Trial-and-error tests showed that σ^2 = 0.01 to 0.001 represents an appropriate final state for RMC with the TiO2 nanoparticles. 500000 RMC cycles were used in each simulation, which guaranteed achieving a minimum residual.

C. XANES spectra calculation

The Ti K-edge XANES spectra of TiO_2 were calculated using a parallel code FDMNES [2007fdmnes]. [its my observation that Feff is better in so called "full multiple scattering mode", but perhaps you tested Feff and didn't like it?-GAW] Two computational methods are available in FDMNES, the multiple scattering (MS) method and the finite-difference method (FDM) [2001Joly, 1999Joly]. The MS method employs the muffin-tin averaging of the potential needed for the expansion of the wave functions. This method is relatively fast in computation, but may not be accurate at photon energies close to the value of the muffin-tin approximation done on the potential [reword?]. The FDM method divides a system into small grids and obtains the wave functions by solving the simultaneous quantum mechanical equations at all the grid points. This removes the assumption of the muffin-tin approximation of the potentials and becomes more accurate in the XANES calculations. However, this method requires significantly greater computational power.

In XANES calculations using FDMNES, the electronic configurations of the atoms of the material are important. The usual initiation technique adopted by FDMNES is to set the appropriate number of "d" electrons, keep the atoms neutral, and put electrons in the large radius 4s or 4p orbitals for a transition metal [2007fdmnes]. In accordance with this we set the electron configuration of Ti as [Ar] $3d^1 4s^2 4p^1$, and that of O as $1s^2 2s^2 2p^4$. [I prsume you used the dipole expansion? -which ought to be good enough-GAW]

For examination of FDMNES, XANES spectra of bulk anatase and bulk rutile were calculated using both the MS and FDM methods, using two atomic cluster radii of 5.6 and 7.0 Å. Crystal symmetry operations were used in the calculations, which reduced the computation time significantly, and is important for use of the FDM method. For calculations of XANES spectra of titania nanoparticles, the structure models obtained from the RMC were employed. The MS method (rather than the FDM method) was used due to the large number of atoms involved in the calculations and the lack of symmetry. A XANES spectrum was calculated with a cluster radius of 7 Å for each Ti atom in a TiO_2 nanoparticle (including both surface and interior Ti atoms). [how did you do the near surface Ti and still get the radius of 7 Å?]The spectra of all the Ti atoms were summed up and averaged for use as the XANES spectrum of the whole nanoparticle.

For comparison, XANES spectra of typical Ti atoms in a TiO_2 nanoparticle were also calculated using the FDM method with a cluster radius of 4 Å, the largest number of atoms we could accomodate. [was this limited by code? Or by our processors?]

D. Structure analysis

The TiO_2 nanoparticle models we generated were analyzed to yield structure characteristics, including the radial-distribution function, coordination numbers as a function of radial distance, bond-length distribution, coordination number of each species, and bond-angle distribution.

The partial radial-distribution function g_{ij} is defined as [1990Vash]

$$g_{ij}(r) = \frac{1}{4\pi r^2 \rho c_j} \cdot \frac{d\langle n_{ij} \rangle}{dr} = \frac{1}{4\pi r^2 N_j} \cdot \frac{d\langle n_{ij} \rangle}{dr} \qquad (5)$$

where r is the radial distance, $d\langle n_{ij} \rangle$ the assemble average of the number of atom j around atom i in a spherical shell with a radius of r and a thickness of dr, ρ the number density of the material ($\rho = N$/volume, where N is the total number of atoms), and c_j the concentration of atom j ($c_j = N_j/N$). g_{ij} represents the probability of finding atom j around atom i at a given radial distance r relative to that at infinitely far away.

The total radial-distribution function g is obtained from

$$g(r) = \sum_{i,j} c_i c_j g_{ij}(r), \qquad (6)$$

and represents the probability of finding one particular atom around any other one at a given radial distance, summed over all possible atom pairings.

The number distribution of atom j around atom i, or the coordination number N_{ij} as a function of r is defined as [1990Vash]

$$N_{ij}(r) = 4\pi c_j \int_0^r g_{ij}(r) r^2 dr \, . \qquad (7)$$

This function represents the assemble-averaged number of atom *j* surrounding atom *i* at a distance *r* between them. At the position of the first shell of atom *j* around atom *i*, N_{ij} equals the coordination number of atom *i* defined in chemistry textbooks.

The coordination number of Ti atoms in bulk anatase, rutile and brookite is 6 and that of O is 3, which is required by the stoichiometry. In amorphous nano-TiO_2, different coordination numbers of Ti and O may present, due both to greatly distorted coordination polyhedra, and the lowered O-Ti coordination for near surface O. The coordination number distributions of Ti and O atoms were also calculated.

The Ti-O bond-length was also calculated for each Ti-O bond in a TiO_2 structure and the corresponding bond-length distribution was obtained. Similarly, the Ti-O-Ti and O-Ti-O bond-angles were also calculated and the corresponding bond-angle distributions obtained.

IV. RESULTS AND DISCUSSION

A. Sample characterization

Fig. 1 shows the XRD pattern of the synthesized TiO_2 sample. It is seen that there are no strong diffraction peaks. Only a few week and broad humps (e.g. the one centered at ~ 35 ^{o}) are present. Given this pattern, the sample is said to be "x-ray amorphous". It cannot be identified as any of the ambient TiO_2 phases (anatase, brookite and rutile), or indeed, as any crystalline structure.

TEM images show that the TiO_2 sample consists of TiO_2 aggregates (~ 0.2 μm in size) (Fig. 2a), which themselves are composed of clots of 2 – 3 nm TiO_2 primary nanoparticles (Fig. 2b). [I'm afraid this TEM image does not convince me. Looks like you are calling noise fluctuations particles. I yield to Jill on this though—if she like it I'm satisfied-GAW]
The primary nanoparticles are ~ 4 – 6 nm apart (Fig. 2b) on the aggregate surface, suggesting that they are loosely aggregated. Selected area electron diffraction of the sample (Fig. 2a insert) also shows no Bragg diffraction maxima.

The specific surface area of the sample determined by using the BET method is 433 m/g^2. This is equivalent to a size of ~ 3.5 nm in diameter assuming that all TiO_2 particles are spherical and that they are isolated from each other. However, the nanoparticles are actually aggregated together, and have contact areas inaccessible to the N_2 gas in the BET determination. As a result, the specific surface area was underestimated and hence the nanoparticles are actually less than 3.5 nm. [I know what you mean but this isn't quite right---the surface area is correctly estimated via BET, it is just that these particles do not have the maximum surface area consistent with their size due to contact. I would say instead something like: Due to the surface contacts the BET must be less than the actual surface area of the analogously separated nanoparticles. Hence the nanoparticle diameters must be somewhat smaller than 3.5 nm. -GAW

These experimental results together establish that the synthesized TiO_2 sample is x-ray amorphous nano-TiO_2 with an average size of 2 – 3 nm in diameter.

B. Generation of structure models from reverse Monte Carlo simulations

The PDF, obtained from the experiments (Fig. 3), reflects the atomic correlations in the amorphous sample. The first intense peak at ~ 1.96 Å corresponds to the closet O shell around a Ti atom. There are several PDF peaks at distances less than 7 Å, representing considerable short-range order in this nominally amorphous sample. At longer radial distances (> ~ 8 Å), the PDF peaks are damped out, indicating lack of long-range order.

Comparisons between some of our calculated and experimental PDFs are illustrated in Fig. 3. The calculated PDF of an as-constructed 2 nm anatase particle (Fig. 3a insert) deviates significantly from the experimental PDF (residue = 41.05; Fig. 3a), while The calculated PDF of a 2 nm anatase particle obtained from MD simulation (Fig. 3b insert) is much closer to the experimental PDF (residue = 6.10; Fig. 3b). The calculated PDF of a 2 nm anatase (Fig. 3c insert) obtained from the RMC procedure (using a MD structure as its input) agrees very well with the experimental PDF (residue = 1.52; Fig. 3c). However, the agreement between the calculated PDF of a 2.5 nm anatase (Fig. 3d insert) obtained from a RMC (using MD structure input) with the experimental PDF is not as good (residue = 3.15; Fig. 3d). Additional trials showed that RMC using an as-constructed anatase nanoparticle as its input (i.e. not one from MD) is unable to generate a PDF consistent with experiment, and we infer this is due the extreme disparity between these structures relative to the adjustment capability of the RMC procedure. These results demonstrate that RMC requires initial inputs from TiO_2 nanoparticle structures defined by MD simulations for adequate convergence, and further that results are sensitive to particle size.

To further investigate the influences of the particle size and the specific phase of an input structure on the RMC output, MD simulations of 2 nm and 3 nm anatase, brookite and rutile nanoparticles were performed to generate initial inputs for the RMC. Fig. 4 shows the comparison between the experimental PDF and the PDF calculated from these RMC-derived structures. Figs. 4a and 4b show that when using the MA potential set [1991Mat] for the MD, the RMC structure derived from a 2 nm anatase particleyields a PDF matching the experimental very well in terms of both the low residual (1.52) and the lack of structure (PDF peaks) at long radial distances (> ~ 8 Å). Though the residuals for the RMC structures derived from 2 nm and 3 nm brookite particles are slightly lower (1.28 and 1.35, respectively), the RMC structures are more crystalline, as seen from the PDF peaks at radial distances > ~ 8 Å. The RMC structures derived from 2 nm and 3 nm rutile particles, and a 3 nm anatase particle have both higher residuals (> 2.0) and significant PDF peaks at > ~ 8 Å.

Figs. 4c and 4d show the PDF of the RMC structures when using the KIM potentials [1996Kim] for the MD. For the 2 nm particles (Fig. 4c), the calculated PDF does not match the experimental one well (residuals > 2.5). The calculated PDF peak at 3 – 4 Å is not well resolved, in contrast to the experimental case. For the 3 nm particles (Fig. 4d), it appears that the RMC structures from brookite and anatase (residuals 1.69 and 1.73, respectively) are equally good in matching the experimental values.

We also attempted RMC with an input structure from MD of a 2 nm anatase particle with a few water molecules adsorbed on the surface. [you should state here how much water?] The RMC process was unable to generate PDF in good agreement with the experimental data in this case.

Hence fromrom RMC refinements, we obtain three RMC structures as candidate models for the nanometer-sized amorphous TiO_2. These are derived from the 2 nm anatase in Fig. 4a and those derived from the 3 nm brookite and 3 nm anatase in Fig. 4d.

C. Selection of structure models by XANES spectra calculations

Experimental Ti K-edge XANES spectra of bulk anatase, bulk rutile and amorphous nano-TiO_2 are shown in Fig. 5. The pre-edge peaks in the range 4965 – 4975 eV are highly sensitive to the coordination environment of Ti atoms [1996Farges]. The pre-edge features will be used to select the best RMC structure models from the amorphous TiO_2 simulations.

For a more detailed examination, we calculated XANES spectra of bulk anatase and bulk rutile (Fig. 6) using varied conditions. Fig. 6 shows that use of an atomic cluster radius of 7.0 Å allows both the MS and FDM methods to reproduce the pre-edge features of the bulk materials, though the FDM method gives better full spectra than the MS method. In bulk titania, the peak A1 is from an electronic quadrupolar t_{2g} transition, A3 from the sum of a dipolar transition and a weak quadrupolar e_g transition, and B from a dipolar transition [1999Joly, 1999Caba]. For bulk anatase (Fig. 6a), calculations using a smaller atomic radius of 5.6 Å were unable to generate the pre-edge features in good agreement with the experimental data.

Fig. 7 shows calculated XANES spectra for several RMC-derived structures. These include the structures starting from 2 nm and 3 nm anatase particles obtained via MD (Fig. 7a), and those starting from 2 nm anatase, brookite and rutile particles obtained from MD (Fig. 7b). Comparing the calculated spectra with the experimental spectra of amorphous nano-TiO_2 (Fig. 7), one sees that the structures from MD of nano-TiO_2 using the KIM potentials [1996Kim] generate larger pre-edge A1 peaks, which correspond to a larger proportion of 4-coordinated Ti atoms in a material [1996Farges]. [note that I also did this same sort of work in a 1987 paper, and it is not just 4-fold coordination, but distortion of the 6 coorinated site in minerals that causes this peak intensification-but I think Farges paper is more thorough-GAW] The calculated spectra for a 3 nm brookite (not shown) is similar to that for the 3 nm anatase shown in Fig. 7a. In contrast, the RMC structures derived from MD of 2 nm TiO_2 nanoparticles using the MAT potentials [1991Mat] produce larger pre-edge A2 peaks (which are associated with 5-coordinated Ti atoms in a material [1996Farges]) with positions and intensities in good agreement with the experimental (Fig. 7).

Combining both the RMC results (above) and the XANES simulations, we conclude that the RMC structure derived from a 2 nm anatase particle by MD using the MAT potentials (Fig. 3c / Fig. 4a) best describes both the WAXS and XAS data. It also appears that the MA set of potentials [1991Mat] is superior to the KIM set [1996Kim] for MD simulations of these types of TiO_2 materials.

D. Analyses of structure models of amorphous nano-TiO_2

We now analyze further the structural features of two models, the one that best describes the WAXS/XAS data (Fig.3c; model 1), and the one from RMC of a 3 nm anatase by MD using the KIM potentials (Fig.4d; model 2). Though the PDF of model 2

is also close to the experimental data (Fig. 4d), the predicted XANES pre-edge feature of model 2 is quite different from the experimental spectra (Fig. 7a), and we wish to determine the basis for this divergence. Figs. 8a and 8b show the 3D and cross-section views of structure model 1; Figs. 8c and 8d show those of structure model 2. [in Fig 8 c it looks like some of the Ti is darker in color than others—any significance to this? GAW]

Figs. 8a and 8b (model 1) reveal that the nano-TiO_2 particle has a strained anatase-like crystalline core, with a dimension of ~ 1 – 2 unit cells, and a highly distorted outer shell, ~ 2 – 4 atomic layers thick. The density of the particle is 3.74 g/cm^3, lower than that of bulk anatase (3.90 g/cm^3). Due to the small dimension of the strained core, x-ray beams are unable to generate coherent reflections in a diffraction experiment. Thus, the synthesized sample appears x-ray amorphous. [this is not actually the reason for the x-ray amorphous result—even highly crystallized particles of this size show only diffuse maxima, indistinguishable from pure Debye diffuse scattering. Of course, the diffusness is even worse for these nanoparticles as the pair correlations are more varied. I actually don't personally like the "x-ray amorphous" label—I'd prefer "lack of Bragg peaks or maxima" or "only diffuse scattered intensity". Ferrihydrite is actually well-crystallized out to 3 nm and its x-ray scattering pattern is completely described only by diffuse scattering. –GAW] The pre-existence of the anatase-like core in the particles may be critical to the development of the amorphous titania into single-phase nano-anatase during heat-treatment. In contrast, the structure shown in Figs. 8c and 8d (model 2) is fully amorphous. [or maybe say, has no crystalline order—what does "fully amorphous" mean anyway? An atomic gas with no pair correlations whatsoever?]

Based on RMC of bulk structure models, Petkov *et al.* concluded that alkoxide-derived amorphous TiO_2 has a brookite-like structure [1998Petkov]. Using a bulk structure model neglects any size effects on the structure. As such, no difference can be made between particle surfaces and interiors, and thus the obtained structure model could be far from realistic.

Fig.9 shows characteristics of the structure models. An obvious difference in the partial radial-distribution function for the two models (Figs. 9a and 9b) is that g(TiTi) is less resolved at ~ 3.3 Å for model 2 (Fig. 9b) than for model 1 (Fig. 9a) due to the non-crystalline structure in model 2. [it is not unrealistic yet, you haven't finished the comparison and gotten to the conclusions yet. GAW] The coordination numbers of Ti, CN(TiO), for model 1 and model 2 are, respectively, 5.3 and 4.1 at the closed O shells (Figs. 9a and 9b). This indicates that the first model TiO_2 is comprised mainly of distorted Ti-O octahedra (CN = 6) and/or pentahedra (CN = 5) rather than tetrahedra (CN = 4), though the Ti-O bond lengths all average about 1.94 Å in the two models (Fig. 9c). More detailed analysis shows that (Fig. 9d), in model 1 some of the Ti atoms are coordinated by 4 O atoms, a few by 7 O atoms, but most Ti atoms are coordinated by 5 and 6 O atoms. In model 2 (Fig. 9d), most Ti atoms are coordinated by 4 O atoms, some are by 5 atoms, and a few are by 3 and 6 atoms (Fig. 9e). Most O atoms are coordinated by 3 and 2 Ti atoms in model 1 (Fig. 9e), while by 2 Ti atoms in model 2 (Fig. 9e).

In a previous study [2007Fern_anaTiO2], Fernandez-Garcia *et al.* concluded that 5 coordinated Ti atoms are present in amorphous TiO_2 according to the pre-edge feature in the XANES spectra. However, their EXAFS fitting showed that Ti atoms are coordinated by 6.2-6.7 oxygen atoms (two shells of O atoms) at a Ti-O distance of 1.71 –

1.92 Å. Their EXAFS results appear inconsistent with their XANES results and are different than our results for model 1.

Figs. 9f and 9g show the bond angle distributions in the two models. The distributions in model 1 can be seen as broadening and overlapping of the distributions in bulk anatase due to distortions of the Ti-O octahedra in the nanoparticles, and truncations of the octahedra at the particle surfaces. [yes, it looks that way to me too-GAW] The distributions in model 2 deviate significantly from those in bulk anatase. This is expected because the model 2 is mainly [how many] comprised of Ti-O tetrahedra in which O-Ti-O angles average around 109 ^{o}.

It is clear that the surface and the interior of a TiO_2 nanoparticle are different in structure (Figs. 8a and 8b). Fig. 10 shows structure characteristics of the surface (the distorted shell) and the core of model 1. From the radial distribution function (Fig. 10a), it is seen that most Ti-O bonds in the core are longer that those in the shell, indicating bond contraction at the surface due to interrupted coordination [this follows from bond valence analysis, i.e. smaller Ti-O CN is consistant with shorter Ti-O bonds-GAW]. The peak Ti-O bond-length of the whole particle is also shorter than that of bulk anatase due to the compression from the effective surface pressure due to small size [1995Tolb]. The reductions in coordination numbers of Ti and O atoms at the surface are clearly seen in Figs. 10b and 10c, while in the core, the coordination numbers are close to those in bulk anatase. Previous studies concluded that the reduction in coordination number of Ti atoms in ultrafine [1997Chen, 1999Chen] or amorphous [1998Luca] titania materials is mainly located on the particle surfaces. Our results are consistent with this. The bond-angle distributions (Figs. 10d and10e) show that those of the whole nanoparticle are largely contributed by the surface atoms—I don't understand this sentence? GAW. These results demonstrate that the structure features of the amorphous TiO_2 nanoparticles are determined dominantly by the surface structure, which is a result of the relaxation of the surface coordination polyhedra to incomplete coordination by oxygen and added degrees of angular freedom. [just a suggestion as an explanation—GAW].

It is clear that model one is the more realistic of the two models, and is consistent with the majority of past work. This model (Figs.8a and 8b) however, provides us with a more detailed understanding of the atomic arrangements in alkoxide-derived nanometer-sized amorphous TiO_2. than previously described. The structure model will be used for future computational study of the mechanical, photonic and catalytic properties of nanometer-sized amorphous titania.

[OK now you have to explain why the XANES of the two models is similar? Otherwise you might not want to bring up the comparison. I expect that the reason is complex and that the intensity of the three peaks in the pre edge vary in a complex way with polyhedral distortion and coordination. Hence there are probably many ensembles of structure types that might give similar pre edge results. Another problem—why are the EXAFS so poorly calculated? Here you probably should have used Feff, and reviewers will ask why you didn't include the chi EXAFS function in the RMC process (its actually a good idea as the EAXFS are Ti centric and would possibly constrain the eventual types of Ti-Ox polyhedra—but I am just guessing, while the Pdf data have all pair correlations. You could, I suppose, also compare the Ti-O and Ti-Ti pair correlations from the models with that from the EXAFS. –GAW]

V. CONCLUSIONS

We examined alkoxide-derived x-ray amorphous titania \composed of ~ 2 nm TiO_2 nanoparticles. The nanoparticles have a highly distorted shell and a strained anatase-like core, with an average Ti-O coordination number of 5.3. The reduction of the coordination number is mainly due to Ti atoms located in the outer shell of the nanoparticle. Most Ti-O bonds (having a mean of 1.940 Å [state std dev]) are shorter than in bulk anatase (four bonds 1.937 Å, two bonds 1.965 Å; average 1.946 Å) [1995Mo], which is due to the bond contractions in the distorted surface shells. -true for all particle this sizes, maybe you could say something different and more apt. se comments earlier-GAW. Because of the existence of the anatase-like cores in the nanoparticles, this type of amorphous nano-TiO_2 serves as an ideal precursor for the synthesis of single-phase nanocrystalline anatase via heat-treatment [2001Nanolett]. Core-shell structures in ultrafine nanoparticles (distorted shells plus strained crystalline cores) may be common in many materials, and have also been observed in small ZnS nanoparticles [2003Nature].

ACKNOWLEDGEMENTS

Synchrotron experiments were performed at beamlines 11-ID-C (WAXS), 12-MB-B (XAS) and 5-BM-D (XAS), Advanced Photon Source, Argonne National Laboratory. We thank Drs. R. Yen and Q. Ma for assistances in the beamline experiments. Computations were carried out in the Geochemistry Computer Cluster, Lawrence Berkeley National Laboratory. Dr. Y. Joly is thanked for helping in using the FDMNES program. Financial support was provided by the U.S. Department of Energy (Grant # DE-FG03-01ER15218 and DE-AC02-05CH11231), as well as the National Science Foundation (Grant # EAR-0123967).

* Corresponding author. E-mail: heng@eps.berkeley.edu.

[1990Vash] P.Vashishta, R. K. Kalia, J. P. Rino and I. Ebbsjo, Phys. Rev. B **41**, 12197 (1990).
[1991Mat] M. Matsui and M. Akaogi, Mol. Simul. **6**, 239 (1991).
[1995Mo] S.-D. Mo and W. Y. Ching, Phys. Rev. B **51**, 13023 (1995).
[1995Tolb] S. H. Tolbert and A. P. Alivisatos, Annu. Rev. Phys. Chem. **46**, 595 (1995).
[1996Farges] F. Farges, G. E. Brown Jr. and J. J. Rehr, Geochim. Cosmochim Acta **60**, 3023 (1996).
[1996Kim] D.-W. Kim, N. Enomoto and Z.-e. Nakagawa, J. Am. Ceram. Soc. **79**, 1095 (1996).
[1997ChenLX_XAFS] L. X. Chen, T. Rajh, Z. Wang and M. C. Thurnauer, J. Phys. Chem. B **101**, 10688 (1997).
[1998JMC] H. Zhang and J. F. Banfield, J. Mater. Chem. **8**, 2073 (1998).

[1998Luca_XAS_TiO2.pdf] V. Luca, S. Djajanti and R. F. Howe, J. Phys. Chem. B **102**, 10650 (1998).
[1998Petk_amoTiO2_Imp-see.pdf] V. Petkov, G. Holzhuter, U. Troge, Th. Gerber and B. Himmel, J. Non-Crystall. Solids **231**, 17 (1998).
[1999AmMiner] H. Zhang and J. F. Banfield, Am. Mineral. **84**, 528 (1999).
[1999Caba] D. Cabaret, Y. Joly, H. Renevier and C. R. Natoli, J. Synchrotron Rad. **6**, 258 (1999).
[1999ChenLX.pdf] L. X. Chen, T. Rajh, W. Jager, J. Nedeljkovic and M. C. Thurnauer, J. Synchrotron Rad. **6**, 445 (1999).
[1999Joly] Y. Joly, D. Cabaret, H. Renevier and C. R. Natoli, Phys. Rev. B. **82**, 2398 (1999).
[2000JMR] H. Zhang and J. F. Banfield, J. Mater. Res. **15**, 437 (2000).
[2000JPCB] H. Zhang and J. F. Banfield, J. Phys. Chem. B **104**, 3481(2000).
[2001dlpoly] W. Smith and T. R. Forster, The DL_POLY v2.13 User Manual (Daresbury Laboratory, Daresbury, Warrington, 2001).
[2001Gao] L. Gao and Q. Zhang, Scr. Mater. **44**, 1195 (2001).
[2001Joly] Y. Joly, Phys. Rev. B **63**, 125120 (2001).
[2001nanolett] H. Zhang, M. Finnegan and J. F. Banfield, Nano Lett. **1**, 81 (2001).
[2002ChemMater] H. Zhang and J. F. Banfield, Chem. Mater. **14**, 4145(2002).
[2002Yeung_TiO2XAS.pdf] K. L. Yeung, A. J. Maira, J. Stolz, E. Hung, N. K.-C. Ho, A. C. Wei, J. Soria, K.-J. Chao and P. L. Yue, J. Phys. Chem. B **106**, 4608 (2002).
[2002Yosh_XAFS.pdf] H. Yoshitake, T. Sugihara and T. Tatsumi, Chem. Mater. **14**, 1023 (2002).
[2003Nature] H. Zhang, B. Gilbert, F. Huang and J. F. Banfield, Nature **424**, 1025 (2003).
[2003Yosh_XAFS.pdf] H. Yoshitake, T. Sugihara and T. Tatsumi, Phys. Chem. Chem. Phys. **5**, 767 (2003).
[2004science] B. Gilbert, F. Huang, H. Zhang, G. A. Waychunas and J. F. Banfield, Science **305**, 651(2004).
[2005JPCB] P. K. Naicker, P. T. Cummings, H. Zhang and J. F. Banfield, J. Phys. Chem. B **109**, 15243 (2005).
[2007fdmnes] Y. Joly, FDMNES User's Guide (Institute Neel, CNRS, Grenoble Cedex, France, 2007).
[2007Fern_anaTiO2] M. Fernandez-Garcia, C. Belver, J. C. Hanson, X. Wang and J. A. Rodriguez, J. Am. Chem. Soc. **129**, 13604 (2007).
[2007JPCC] H. Zhang and J. F. Banfield, J. Phys. Chem. C **111**, 6621 (2007).

Figure captions

FIG.1. (Color online) XRD pattern of nanometer-sized amorphous TiO_2. Diffraction data (in relative intensities) from the ICDD database for three ambient TiO_2 phases, anatase (Ref. Code. 00-021-1272), brookite (Ref. Code. 00-029-1360) and rutile (Ref. Code. 00-021-1276) are also shown for comparison.

FIG. 2. TEM images of nanometer-sized TiO_2. (a) Low resolution image showing aggregate sizes are ~ 2 μm in diameter. Insert: selected area electron diffraction pattern. (b) High resolution image showing primary particles are ~ 2 – 3 nm in diameter. Bottom: integration of brightness showing TiO_2 nanoparticles are ~ 4 – 6 nm apart on aggregate surface.

FIG. 3. (Color online) Comparison between experimental PDF of amorphous nano-TiO_2 and those calculated for anatase particles: (a) as-constructed (unrelaxed), 2 nm; (b) from MD, 2 nm; (c) from RMC, 2 nm; and (d) from RMC, 2.5 nm. Input structures for the RMC were from MD using the MA interatomic potentials **[1991Mat].** Inserts show structure models used for the PDF calculations.

FIG. 4. (Color online) Comparison between experimental PDF of amorphous nano-TiO_2 and those calculated from RMC structures. Input structures for the RMC were from MD of (a, c) 2 nm and (b, d) 3 nm TiO_2 particles using the MA interatomic potentials (a, b) **[1991Mat]** and the KIM potentials (c, d) **[1996Kim]**.

FIG. 5. (Color online) Experimental XANES spectra of bulk anatase, bulk rutile and amorphous nano-TiO_2.

FIG. 6. (Color online) Comparison of calculated XANES spectra of (a) bulk anatase and (b) bulk rutile with the experimental spectra. Finite difference method (FDM) and multiple scattering (MS) method were used in the calculations with two atomic cluster radii (R) of 5.6 Å and 7.0 Å. Characteristic peaks are shown on the experimental spectra.

FIG. 7. (Color online) Comparison of calculated XANES spectra of nano-TiO_2 with the experimental spectra of amorphous nano-TiO_2. MS method (cluster radius 7.0 Å) and FDM method (cluster radius 4.0 Å) were used in the calculations. Structure models for the spectra calculations were from RMC with input structures from MD of (a) 2 nm and 3 nm anatase particles, and (b) 2 nm anatase, brookite and rutile particles (all with MS method). The MA **[1991Mat]** and KIM **[1996Kim]** interatomic potentials were used in the MD.

FIG. 8. (Color online) Structure of a TiO_2 nanoparticle generated by RMC of (a, b) a ~ 2 nm anatase particle (model 1), and (c, d) a ~ 3 nm anatase particle (model 2). (b, d) are cross-section views. Input structures for the RMC were from MD using the MA interatomic potentials **[1991Mat]** (a, b) and the KIM potentials **[1996Kim]** (c, d). Ti: smaller balls; O: bigger balls.

FIG. 9. (Color online) Structure characteristics of amorphous nano-TiO_2. (a) RDF and CN of model 1. g-total RDF, g(AB) – partial RDF of B around A, CN(AB) – CN of B around A. (b) RDF and CN of model 2. (c) Bond length distribution. (d) Coordination number distribution of Ti. (e) Coordination number distribution of O. (f) Ti-O-Ti bond angle distribution. (g) O-Ti-O bond angle distribution. Vertical lines represent the corresponding values in bulk anatase (shown in relative magnitudes).

FIG. 10. (Color online) Structure characteristics on the surface, in the core and in the whole particle of amorphous nano-TiO_2 (model 1). (a) RDF of O around Ti. (b) Coordination number distribution of Ti. (c) Coordination number distribution of O. (d) Ti-O-Ti bond angle distribution. (e) O-Ti-O bond angle distribution. Vertical lines represent the corresponding values in bulk anatase (shown in relative magnitudes).

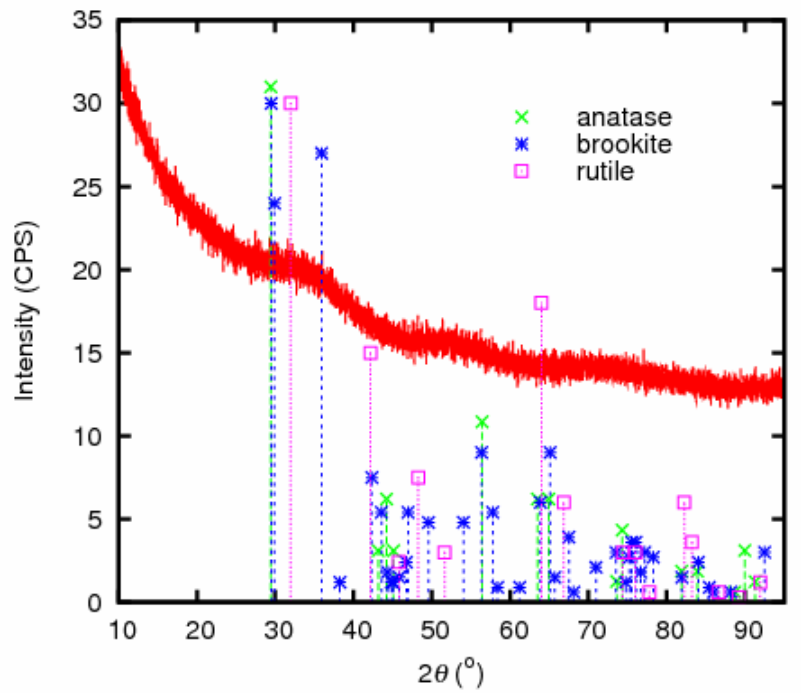

FIG.1. (Color online) XRD pattern of nanometer-sized amorphous TiO_2. Diffraction data (in relative intensities) from the ICDD database for three ambient TiO_2 phases, anatase (Ref. Code. 00-021-1272), brookite (Ref. Code. 00-029-1360) and rutile (Ref. Code. 00-021-1276) are also shown for comparison.

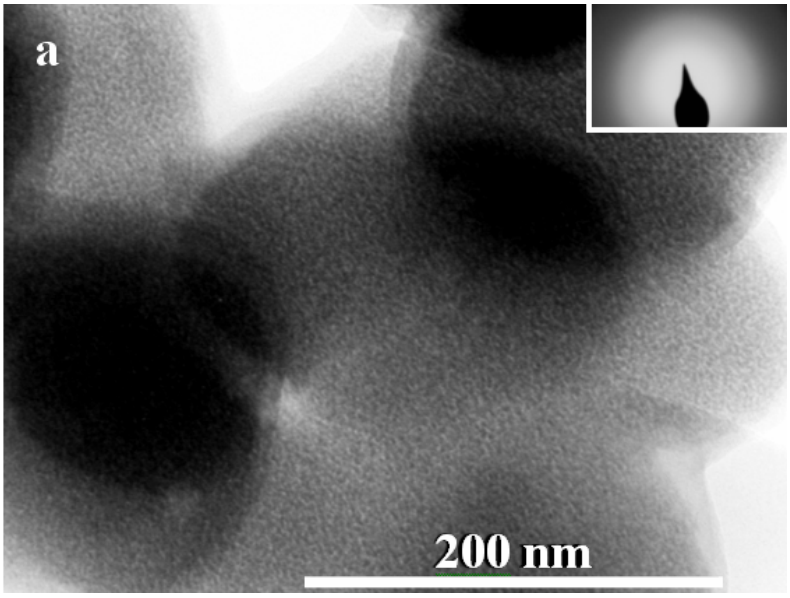

(FIG.2a)

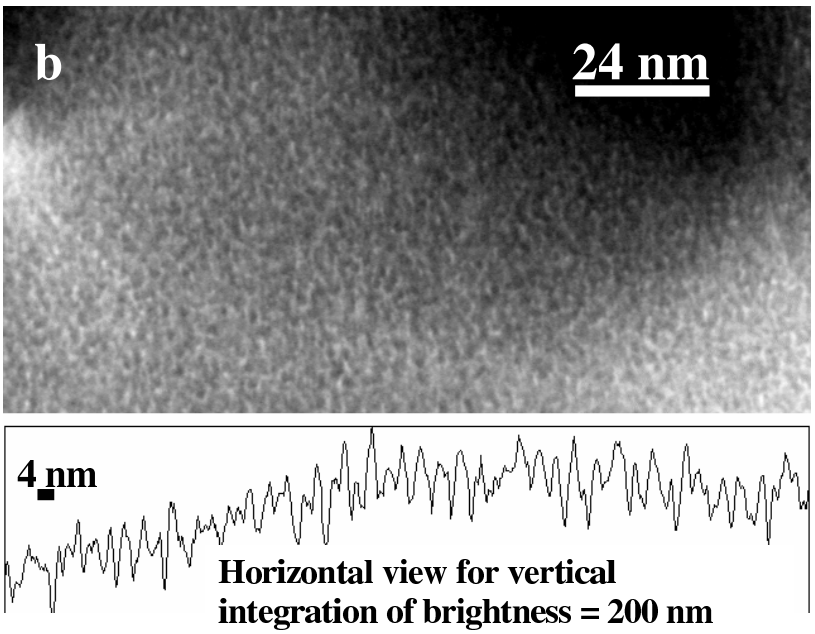

(FIG. 2b)

FIG. 2. TEM images of nanometer-sized TiO_2. (a) Low resolution image showing aggregate sizes are ~ 2 μm in diameter. Insert: selected area electron diffraction pattern. (b) High resolution image showing primary particles are ~ 2 – 3 nm in diameter. Bottom: integration of brightness showing TiO_2 nanoparticles are ~ 4 – 6 nm apart on aggregate surface.

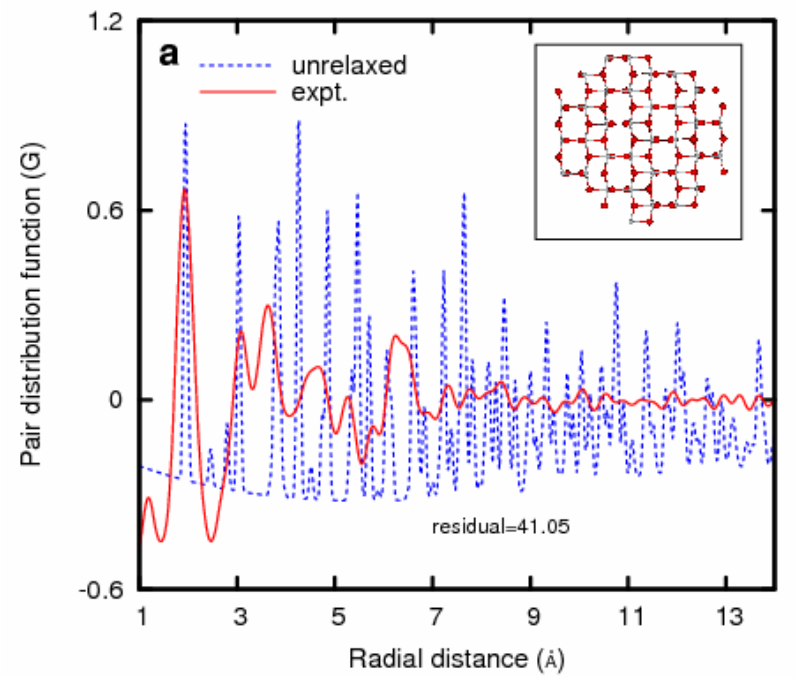

(FIG. 3a)

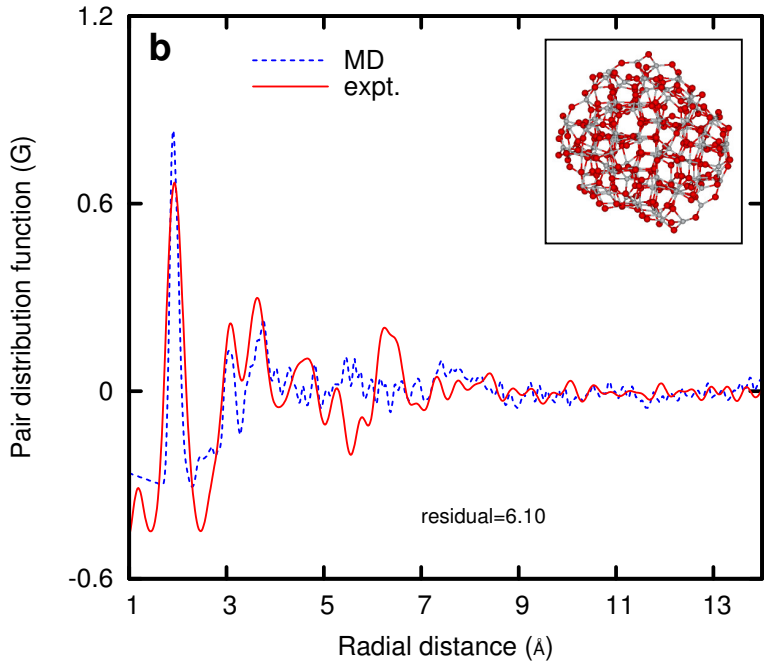
b
MD
expt.
residual=6.10
Pair distribution function (G)
Radial distance (Å)
1.2
0.6
0
-0.6
1
3
5
7
9
11
13

(FIG. 3b)

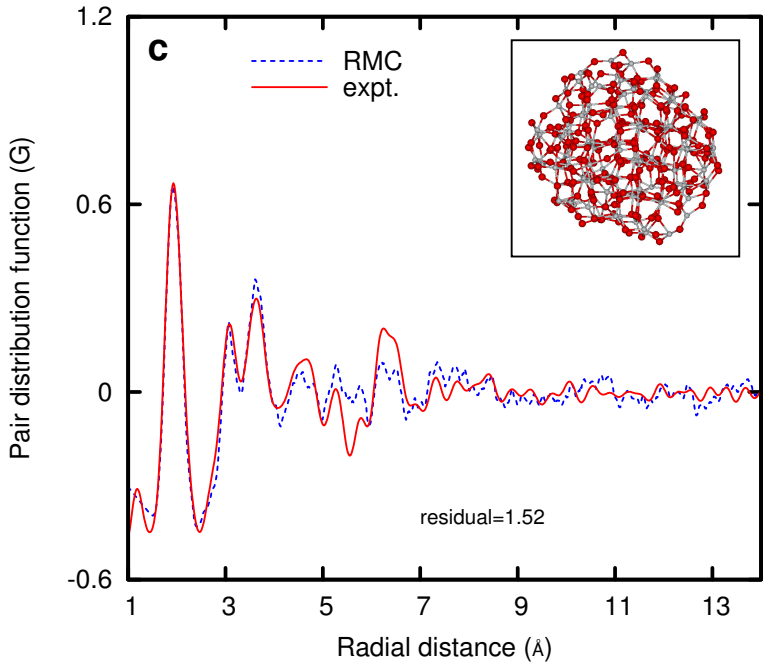
c
RMC
expt.
residual=1.52
Pair distribution function (G)
Radial distance (Å)
1.2
0.6
0
-0.6
1
3
5
7
9
11
13

(FIG. 3c)

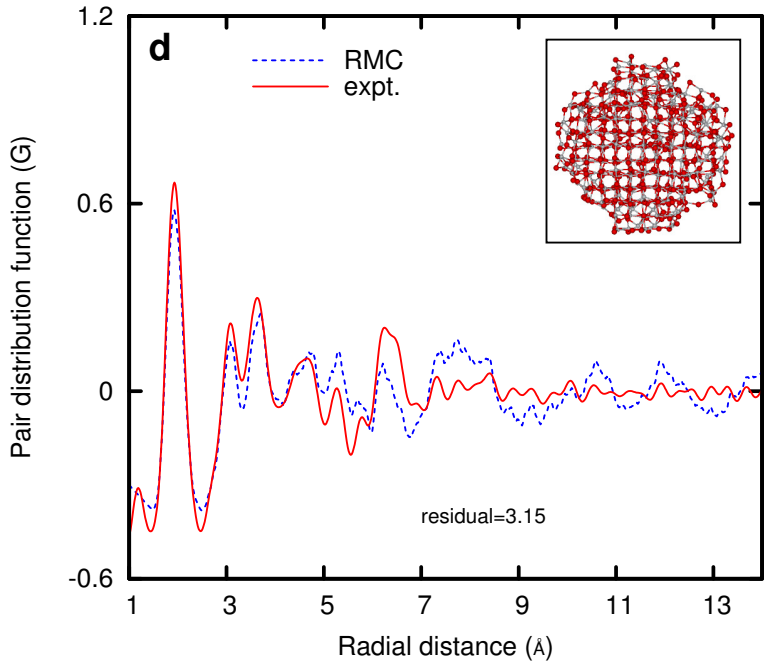

(FIG. 3d)

FIG. 3. (Color online) Comparison between experimental PDF of amorphous nano-TiO_2 and those calculated for anatase particles: (a) as-constructed (unrelaxed), 2 nm; (b) from MD, 2 nm; (c) from RMC, 2 nm; and (d) from RMC, 2.5 nm. Input structures for the RMC were from MD using the MA interatomic potentials **[1991Mat].** Inserts show structure models used for the PDF calculations.

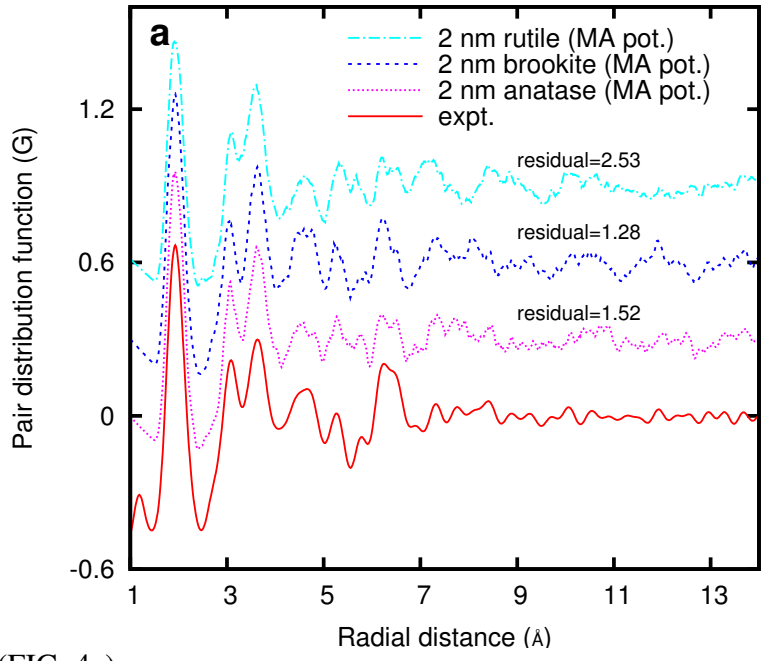

(FIG. 4a)

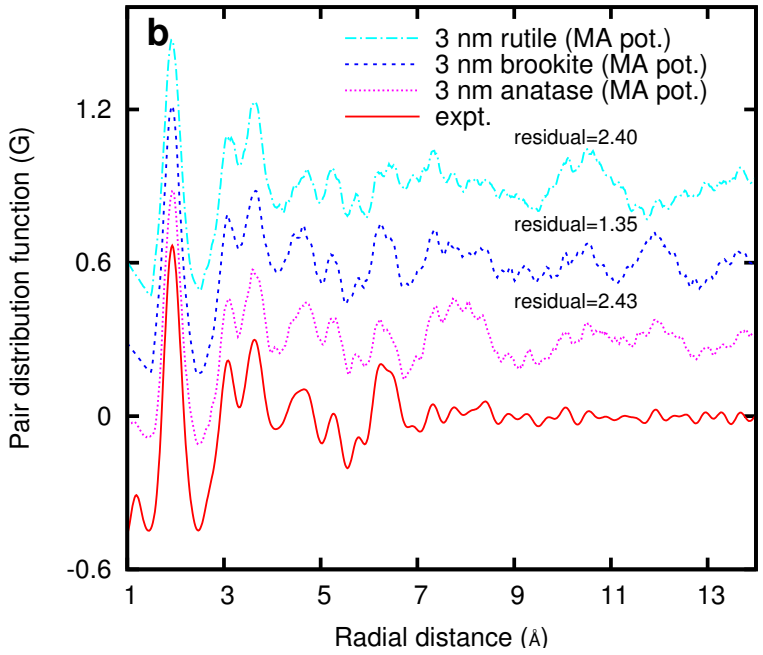
b
3 nm rutile (MA pot.)
3 nm brookite (MA pot.)
3 nm anatase (MA pot.)
expt.
residual=2.40
residual=1.35
residual=2.43
Pair distribution function (G)
1.2
0.6
0
-0.6
1
3
5
7
9
11
13
Radial distance (Å)

(FIG. 4b)

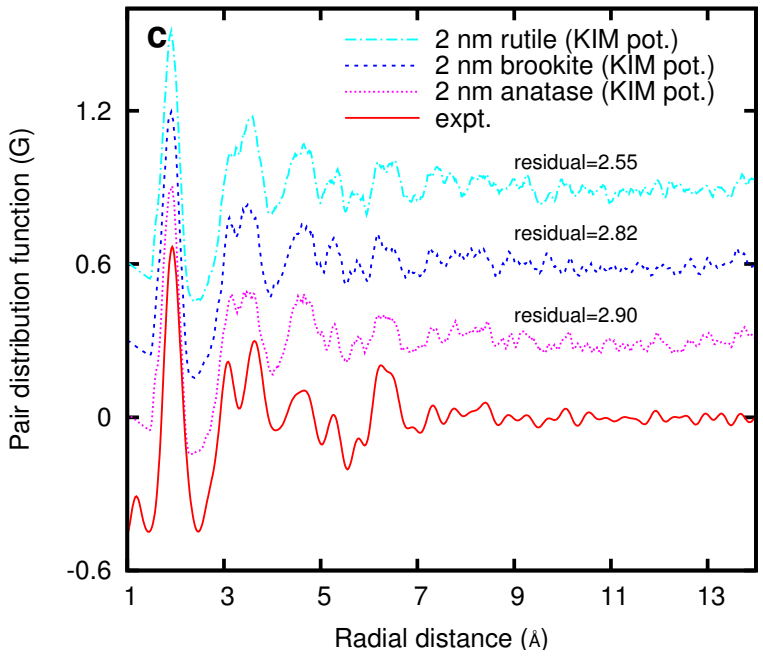
c
2 nm rutile (KIM pot.)
2 nm brookite (KIM pot.)
2 nm anatase (KIM pot.)
expt.
residual=2.55
residual=2.82
residual=2.90
Pair distribution function (G)
1.2
0.6
0
-0.6
1
3
5
7
9
11
13
Radial distance (Å)

(FIG. 4c)

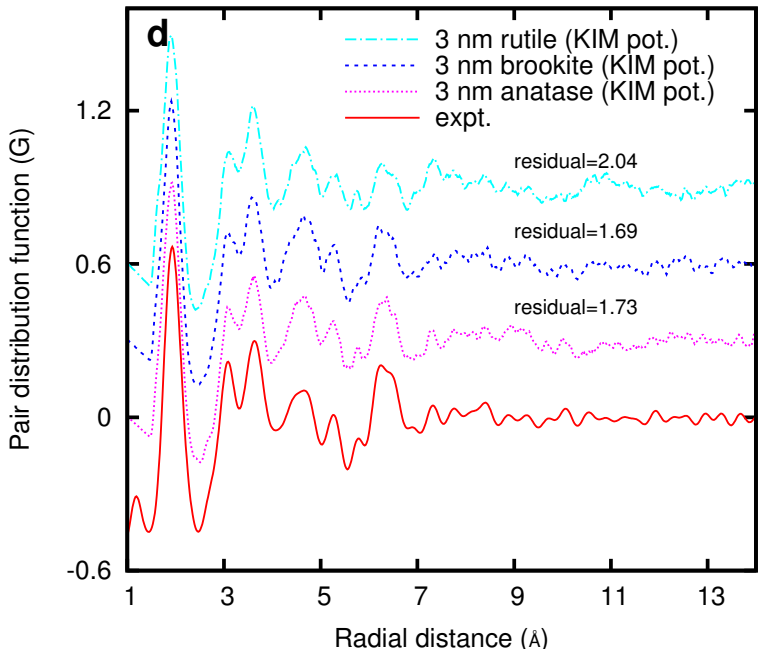

(FIG. 4d)

FIG. 4. (Color online) Comparison between experimental PDF of amorphous nano-TiO_2 and those calculated from RMC structures. Input structures for the RMC were from MD of (a, c) 2 nm and (b, d) 3 nm TiO_2 particles using the MA interatomic potentials (a, b) **[1991Mat]** and the KIM potentials (c, d) **[1996Kim]**.

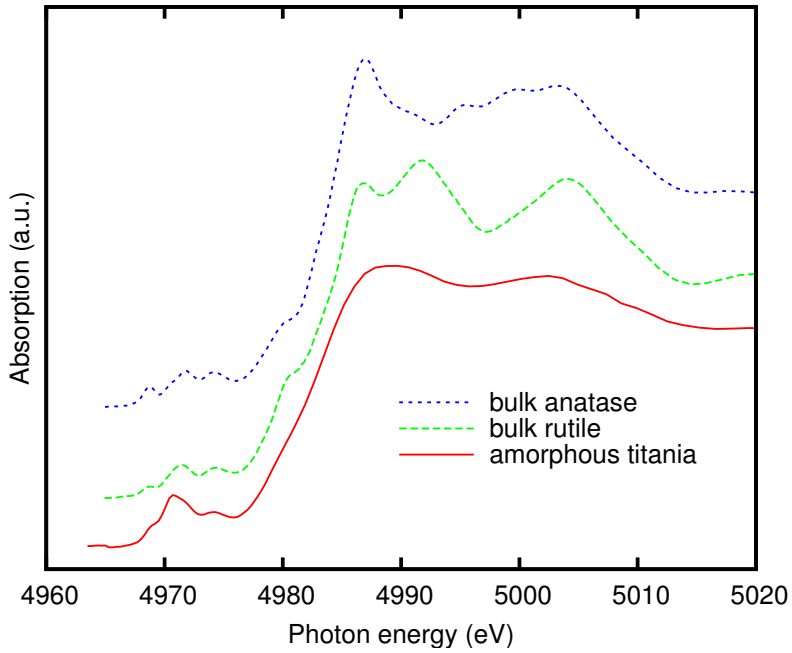

FIG. 5. (Color online) Experimental XANES spectra of bulk anatase, bulk rutile and amorphous nano-TiO_2.

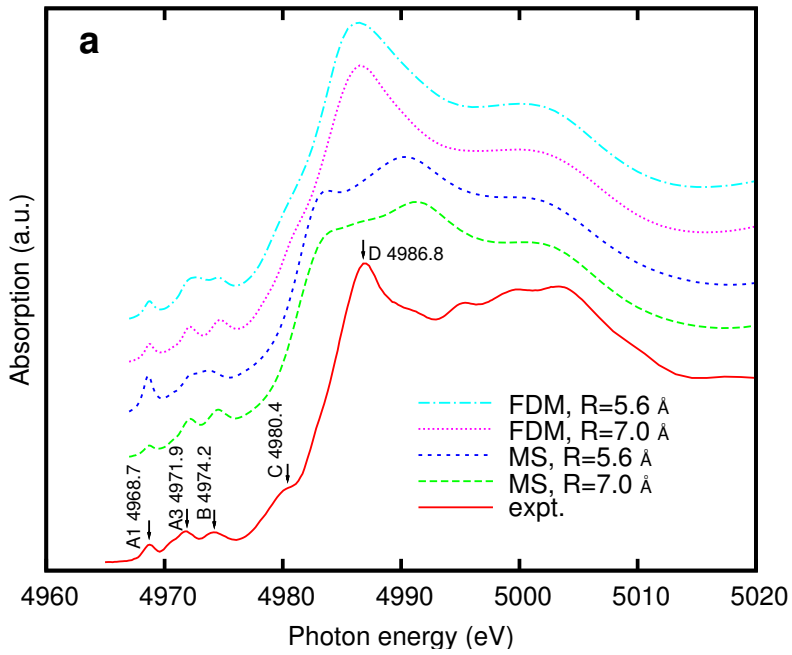

(FIG. 6a)

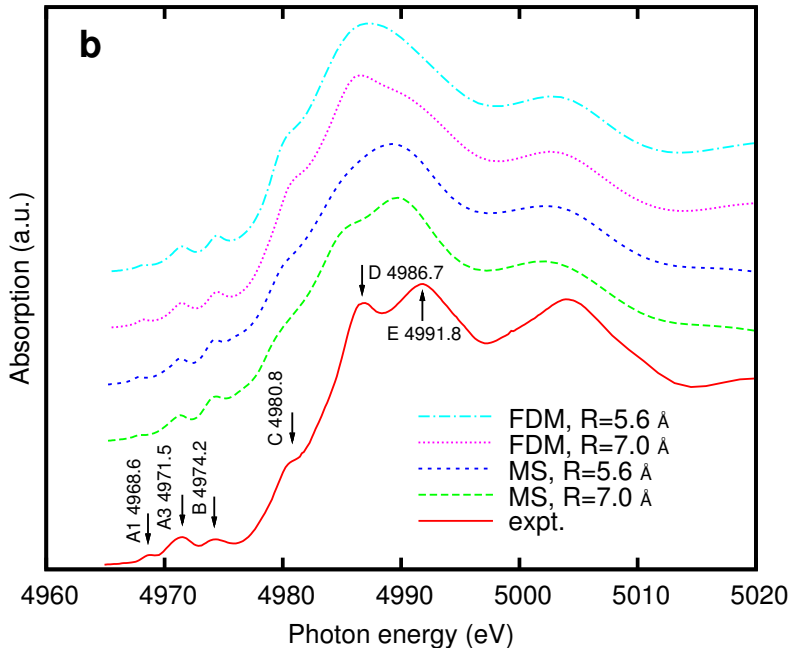

(FIG. 6b)

FIG. 6. (Color online) Comparison of calculated XANES spectra of (a) bulk anatase and (b) bulk rutile with the experimental spectra. Finite difference method (FDM) and multiple scattering (MS) method were used in the calculations with two atomic cluster radii (R) of 5.6 Å and 7.0 Å. Characteristic peaks are shown on the experimental spectra.

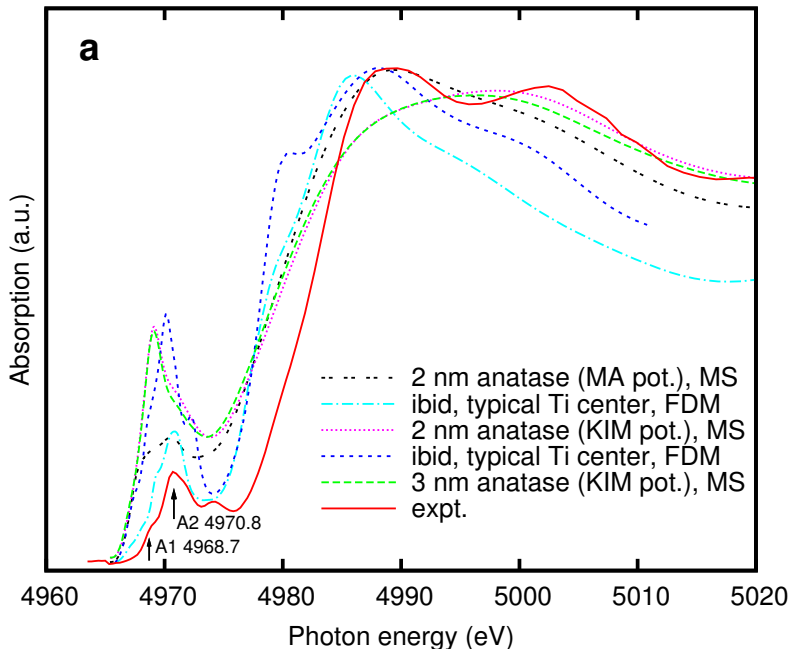

(FIG. 7a)

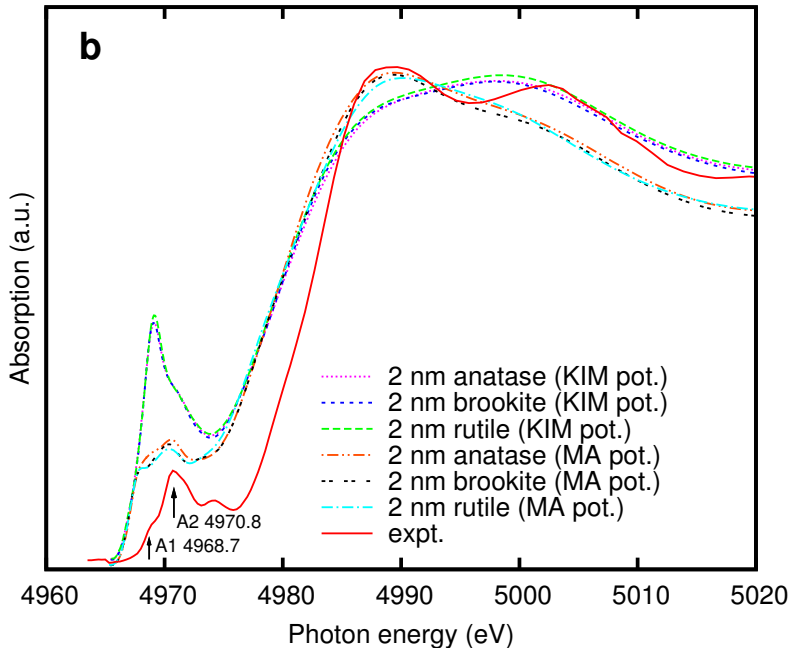

(FIG. 7b)

FIG. 7. (Color online) Comparison of calculated XANES spectra of nano-TiO_2 with the experimental spectra of amorphous nano-TiO_2. MS method (cluster radius 7.0 Å) and FDM method (cluster radius 4.0 Å) were used in the calculations. Structure models for the spectra calculations were from RMC with input structures from MD of (a) 2 nm and 3 nm anatase particles, and (b) 2 nm anatase, brookite and rutile particles (all with MS method). The MA **[1991Mat]** and KIM **[1996Kim]** interatomic potentials were used in the MD.

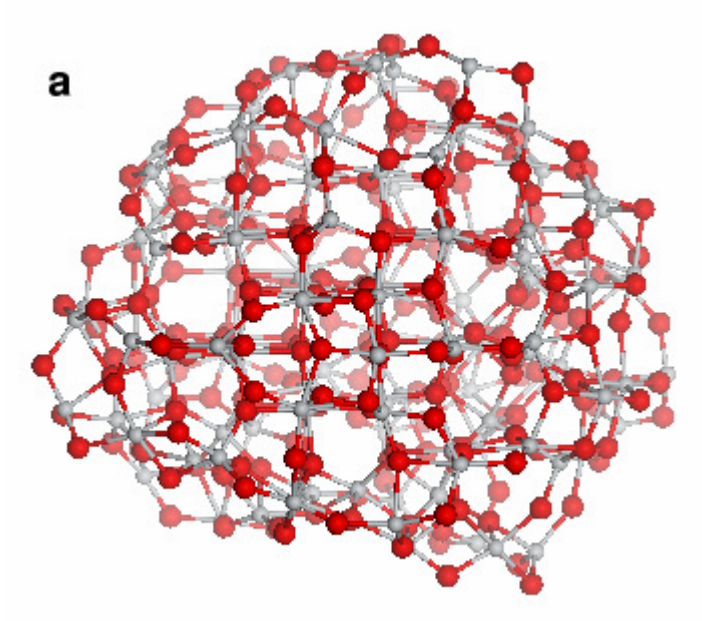

(FIG. 8a)

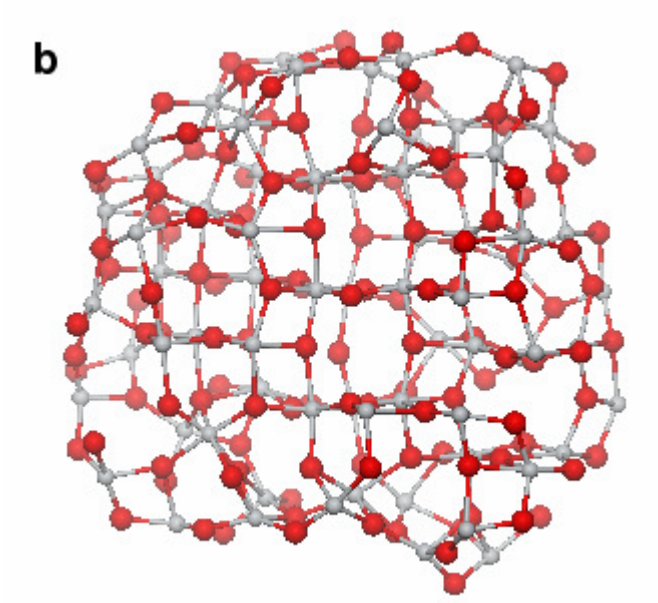

(FIG. 8b)

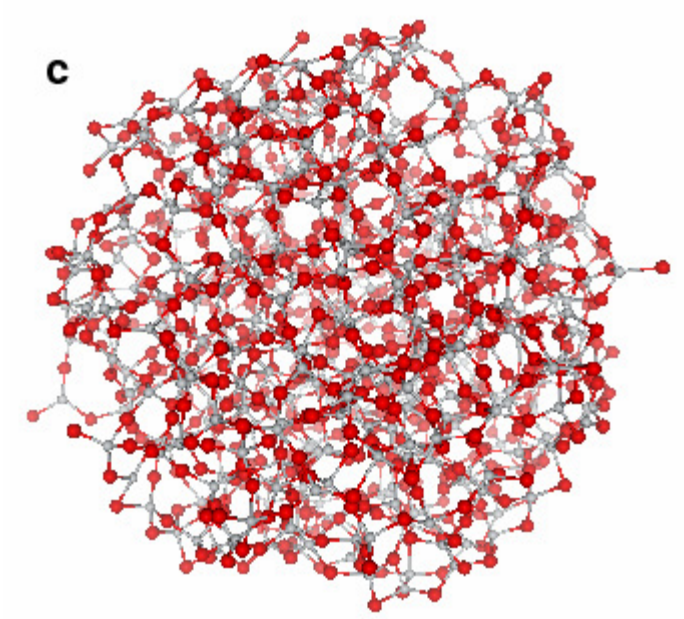

(FIG. 8c)

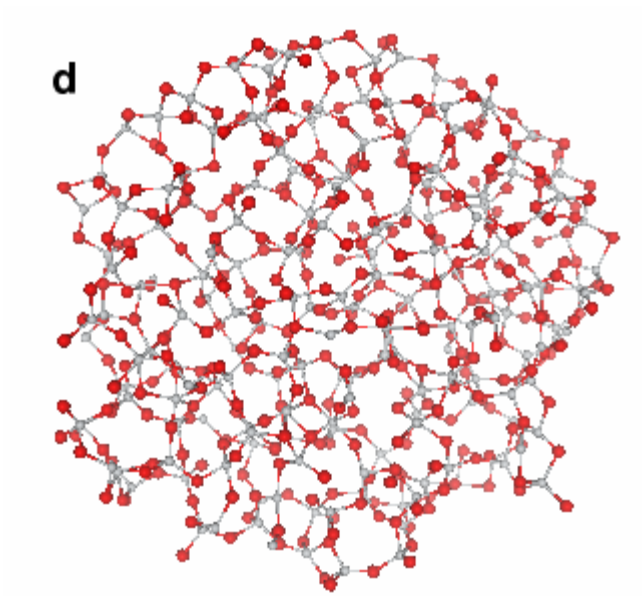

(FIG. 8d)

FIG. 8. (Color online) Structure of a TiO_2 nanoparticle generated by RMC of (a, b) a ~ 2 nm anatase particle (model 1), and (c, d) a ~ 3 nm anatase particle (model 2). (b, d) are cross-section views. Input structures for the RMC were from MD using the MA interatomic potentials **[1991Mat]** (a, b) and the KIM potentials **[1996Kim]** (c, d). Ti: smaller balls; O: bigger balls.

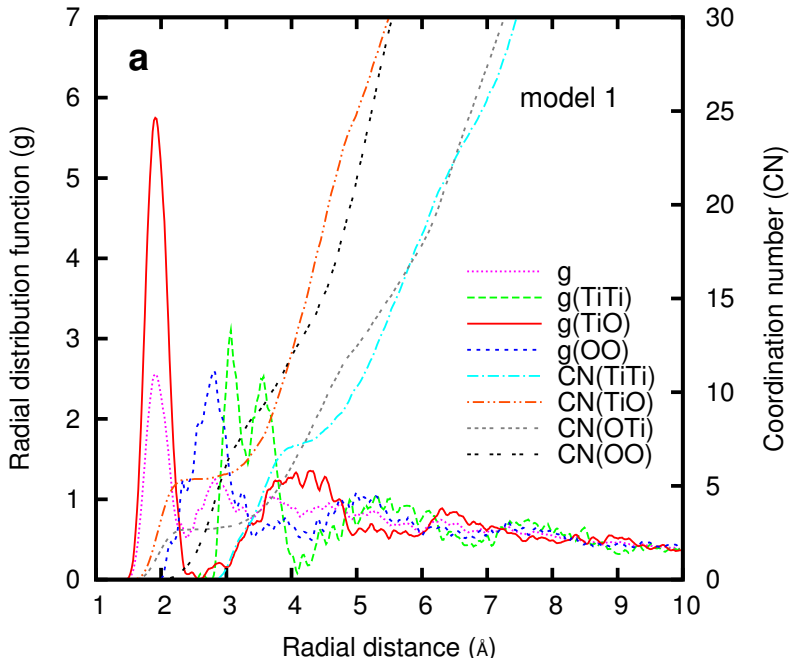
a
model 1
g
g(TiTi)
g(TiO)
g(OO)
CN(TiTi)
CN(TiO)
CN(OTi)
CN(OO)
Radial distribution function (g)
Coordination number (CN)
Radial distance (Å)

(FIG. 9a)

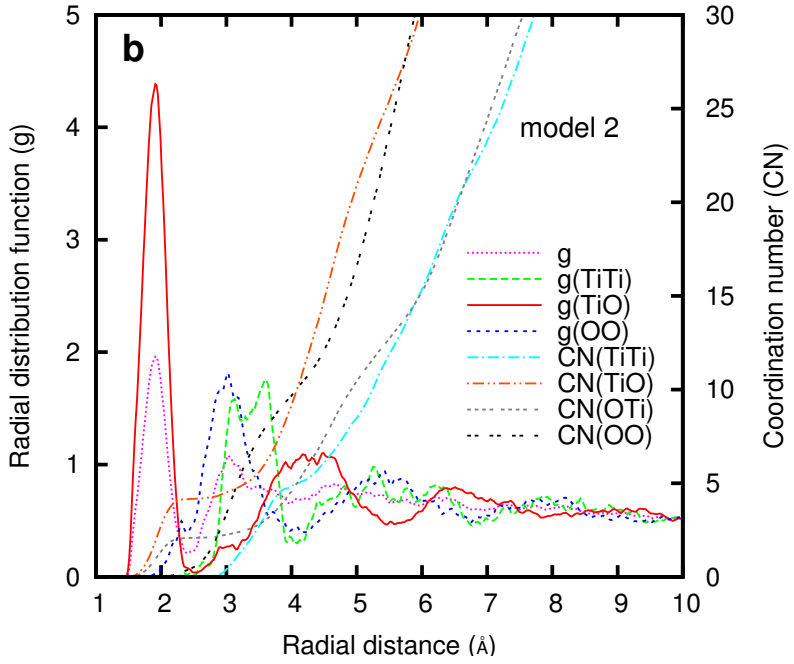
b
model 2
g
g(TiTi)
g(TiO)
g(OO)
CN(TiTi)
CN(TiO)
CN(OTi)
CN(OO)
Radial distribution function (g)
Coordination number (CN)
Radial distance (Å)

(FIG. 9b)

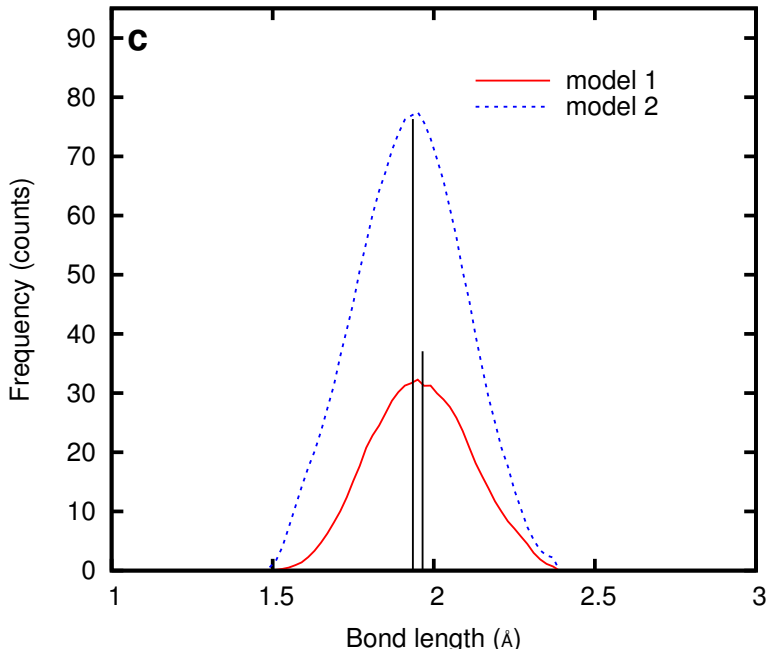
c
model 1
model 2
Frequency (counts)
Bond length (Å)
0
10
20
30
40
50
60
70
80
90
1
1.5
2
2.5
3

(FIG. 9c)

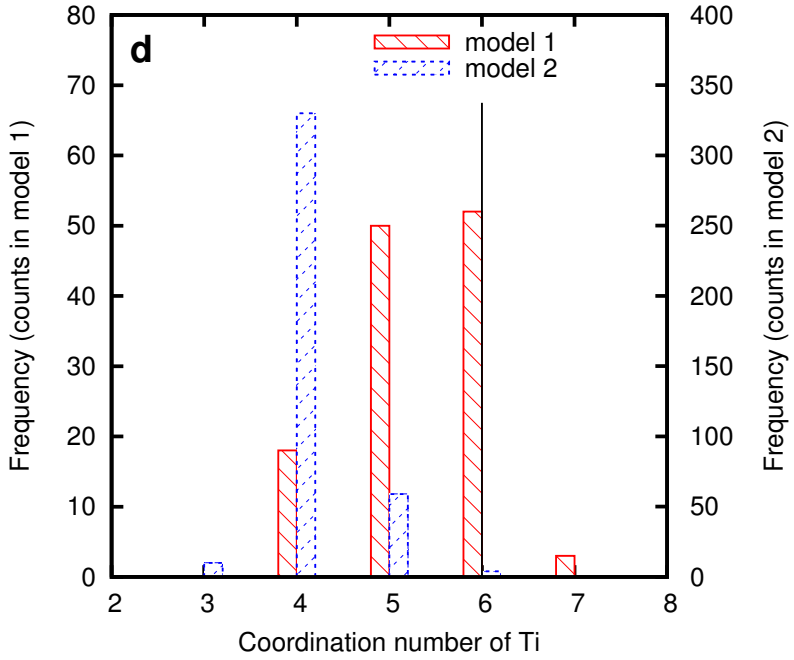
d
model 1
model 2
Frequency (counts in model 1)
Frequency (counts in model 2)
Coordination number of Ti
0
10
20
30
40
50
60
70
80
0
50
100
150
200
250
300
350
400
2
3
4
5
6
7
8

(FIG. 9d)

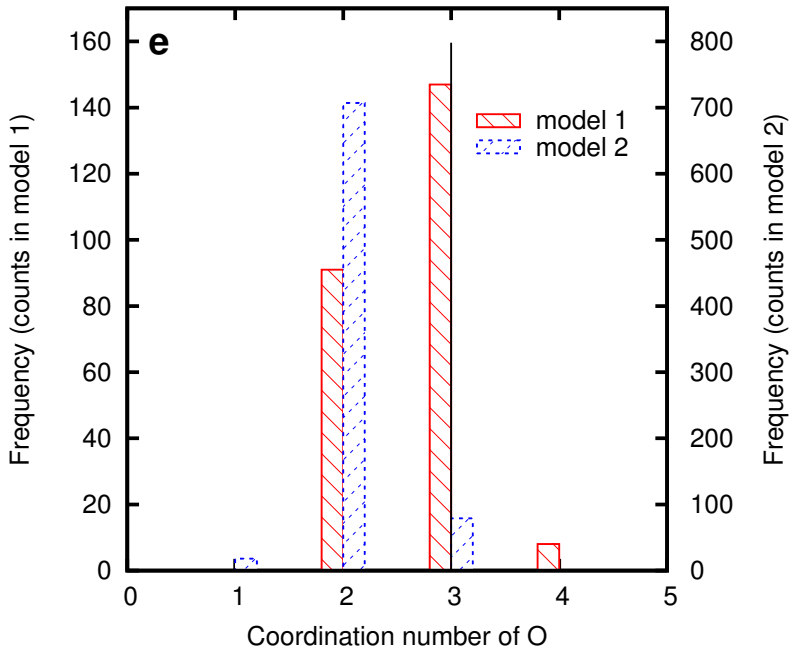
e
model 1
model 2
Frequency (counts in model 1)
Frequency (counts in model 2)
Coordination number of O
0
20
40
60
80
100
120
140
160
0
100
200
300
400
500
600
700
800
0
1
2
3
4
5

(FIG. 9e)

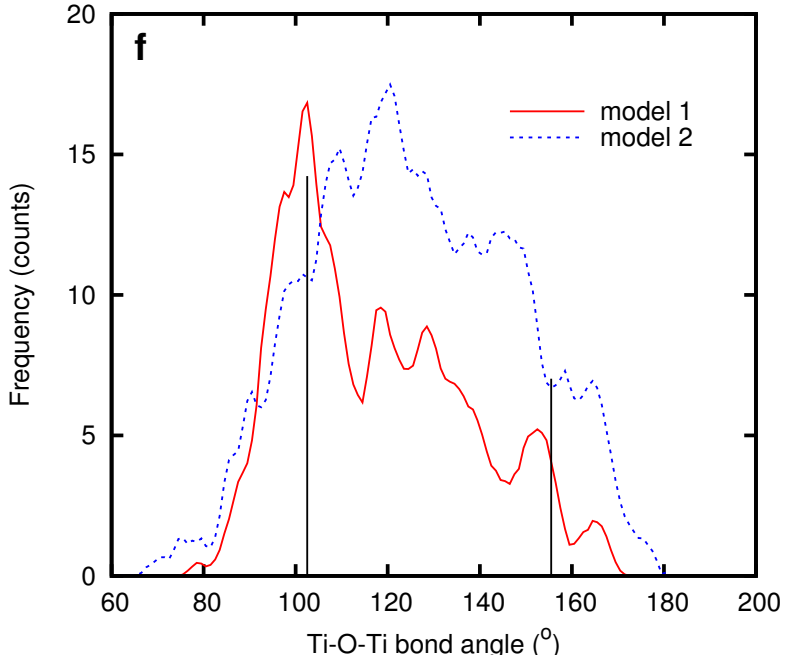
f
model 1
model 2
Frequency (counts)
Ti-O-Ti bond angle (°)
0
5
10
15
20
60
80
100
120
140
160
180
200

(FIG. 9f)

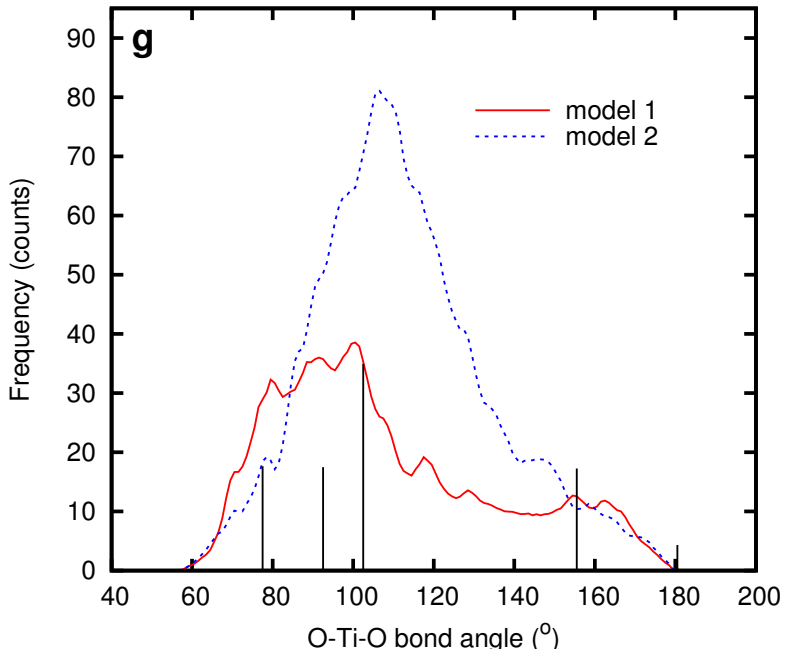

(FIG. 9g)

FIG. 9. (Color online) Structure characteristics of amorphous nano-TiO_2. (a) RDF and CN of model 1. g-total RDF, g(AB) – partial RDF of B around A, CN(AB) – CN of B around A. (b) RDF and CN of model 2. (c) Bond length distribution. (d) Coordination number distribution of Ti. (e) Coordination number distribution of O. (f) Ti-O-Ti bond angle distribution. (g) O-Ti-O bond angle distribution. Vertical lines represent the corresponding values in bulk anatase (shown in relative magnitudes).

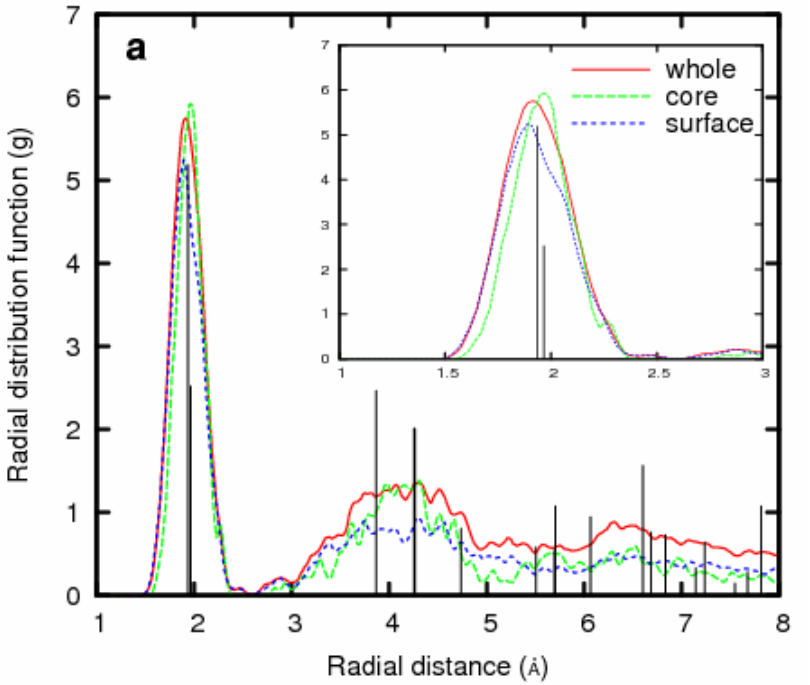

(FIG. 10a)

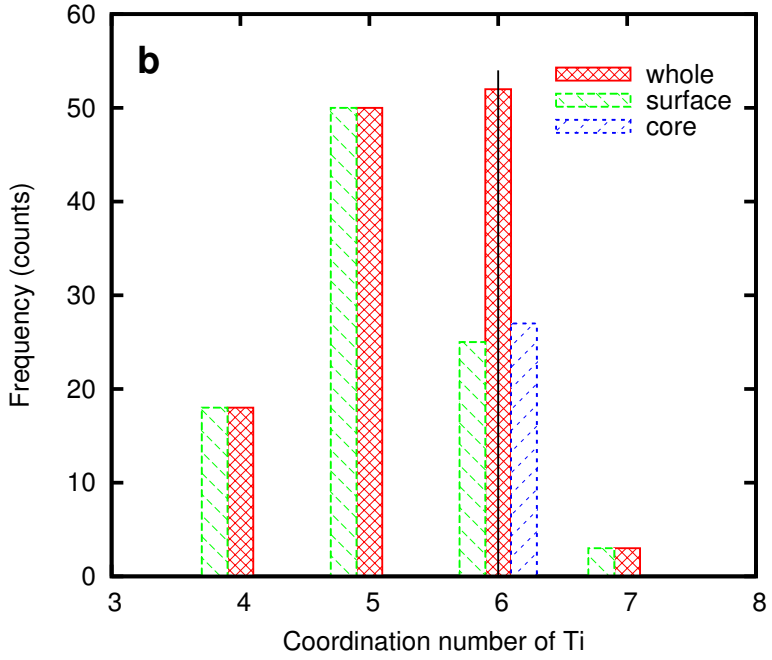

(FIG. 10b)

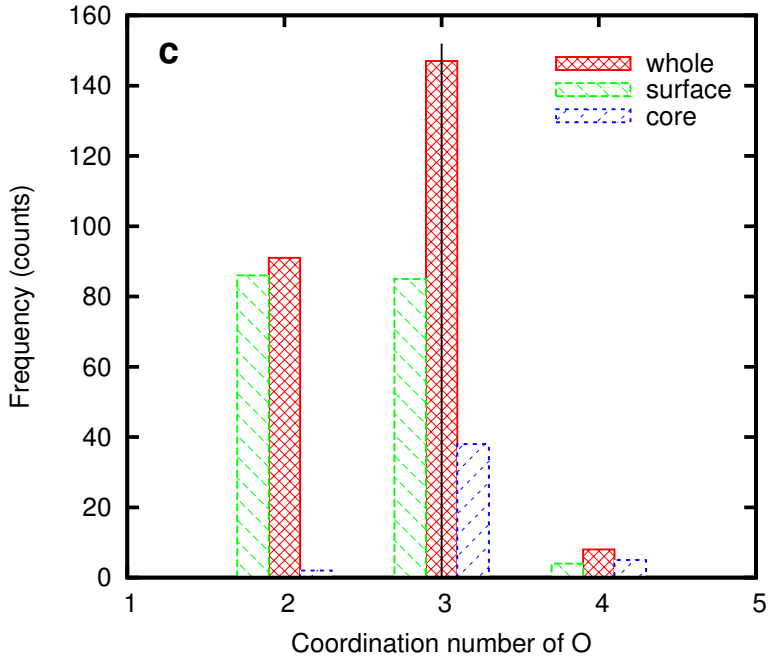

(FIG. 10c)

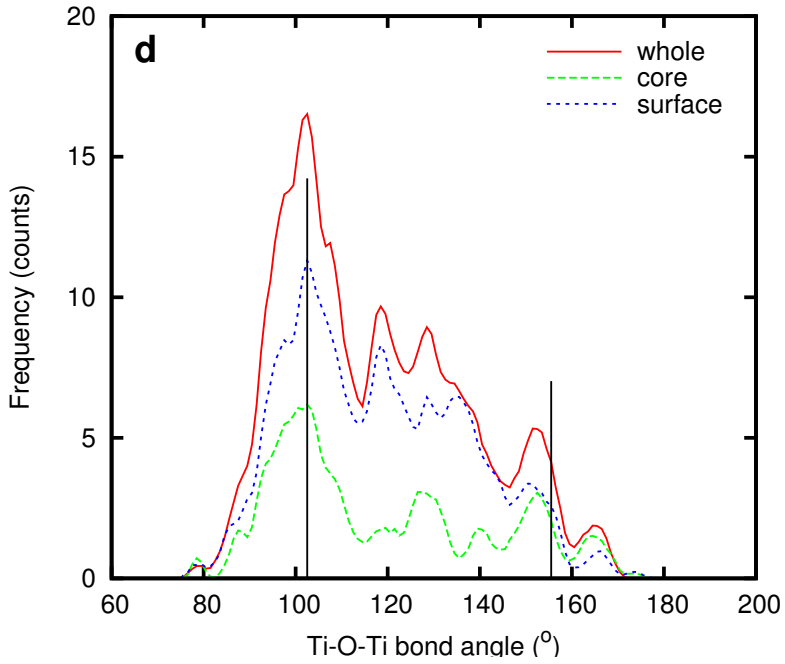

(FIG. 10d)

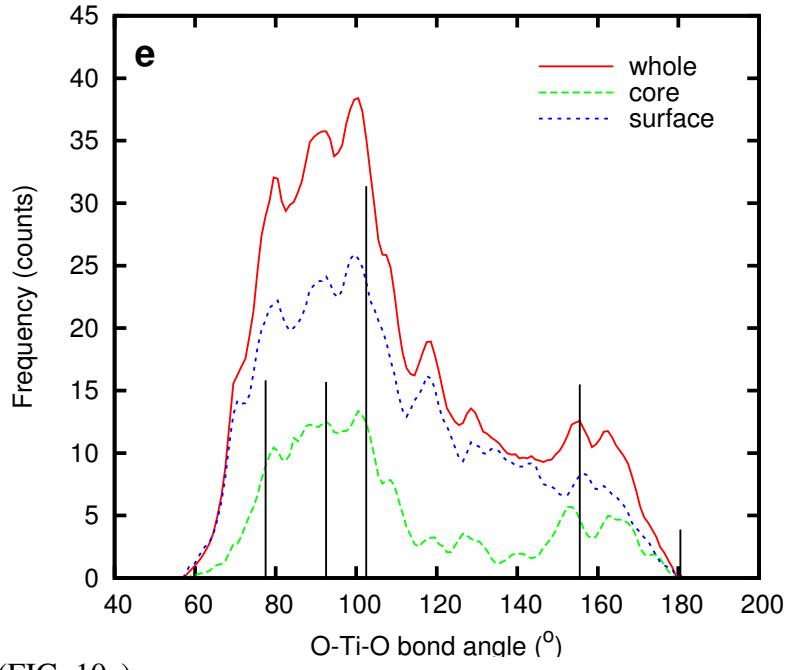

(FIG. 10e)

FIG. 10. (Color online) Structure characteristics on the surface, in the core and in the whole particle of amorphous nano-TiO_2 (model 1). (a) RDF of O around Ti. (b) Coordination number distribution of Ti. (c) Coordination number distribution of O. (d) Ti-O-Ti bond angle distribution. (e) O-Ti-O bond angle distribution. Vertical lines represent the corresponding values in bulk anatase (shown in relative magnitudes).